Agricultural and Forest Meteorology 218–219 (2016) 50–64

Contents lists available at ScienceDirect

Agricultural and Forest Meteorology

journal homepage: www.elsevier.com/locate/agrformet

Contrasting changes in gross primary productivity of different regions of North America as affected by warming in recent decades

Zelalem A. Mekonnen[a,*], Robert F. Grant[a], Christopher Schwalm[b]

[a] Department of Renewable Resources, University of Alberta, Edmonton, Canada T6G 2E3
[b] Woods Hole Research Center, Falmouth, MA 02540, USA

ARTICLE INFO

Article history:
Received 13 May 2015
Received in revised form 10 October 2015
Accepted 23 November 2015
Available online 17 December 2015

Keywords:
Ecosys
Ecosystem modeling
Warming
North America GPP
Carbon flux

ABSTRACT

Ecosystem responses to the increasing warming in recent decades across North America (NA) are spatially heterogeneous and partly uncertain. Here we examined the spatial and temporal variability of warming across different eco-regions of NA using long-term (1979–2010) climate data (North America Regional Reanalysis (NARR)) with 3-hourly time-step and 0.25° × 0.25° spatial resolution and run a comprehensive mathematical process model, *ecosys* to study the impacts of this variability in warming on gross primary productivity (GPP). In a site scale test of model results, annual GPP modeled for pixels which corresponded to the locations of 20 eddy covariance flux towers correlated well (R^2 = 0.76) with annual GPP derived from the towers in 2005. At continental scale, long-term annual average modeled GPP correlated well (geographically weighed regression R^2 = 0.8) with MODIS GPP. GPP modeled in eastern temperate forests and most areas with lower mean annual air temperature (T_a), such as those in northern forests and Taiga, increased due to early spring and late autumn warming observed in NARR and these eco-regions contributed 92% of the increases in NA GPP over the last three decades. However, modeled GPP declined in most southwestern regions of NA (accounting >50% of the ecosystems with declining GPP), due to water stress from rising T_a and declining precipitation, implying that further warming and projected dryness in this region could further reduce NA carbon uptake. Overall, NA modeled GPP increased by 5.8% in the last 30 years, with a positive trend of +0.012 ± 0.01 Pg C yr^{-1} and a range of −1.16 to +0.87 Pg C yr^{-1} caused by interannual variability of GPP from the long-term (1980–2010) mean. This variability was the greatest in southwest of US and part of the Great Plains, which could be as a result of frequent El Niño–Southern Oscillation' events that led to major droughts.

1. Introduction

There is widespread evidence that ecosystems are responding to warming in recent decades. Increase in the length of growing season has been reported by several studies using the Normalized Difference Vegetation Index (NDVI) in different regions: northern hemisphere (Kim et al., 2012), North America (NA) (White et al., 2009; Zhu et al., 2012), northern higher latitudes (McManus et al., 2012; Myneni et al., 1997; Olthof et al., 2008; Tucker et al., 2001; Verbyla, 2008; Zhang et al., 2008). NDVI values are strongly correlated to photosynthetically active radiation absorbed by vegetation. Increasing NDVI values indicating increasing vegetation density and gross primary productivity (GPP) (Box et al., 1989) over time in northern higher latitudes have been reported in some studies (Myneni et al., 1997; White et al., 2009). Evidence of increases in vegetation cover and northward movement of the tree line in northern higher latitudes has also been reported in several studies (Beck et al., 2011; Swann et al., 2010; Van Bogaert et al., 2011). In contrast, a study in southwest US reported a decline in productivity as a result of warming (Williams et al., 2010).

Warming affects GPP and ecosystem respiration (R_e) which are the major components of carbon exchange between the terrestrial ecosystem and the atmosphere (Albert et al., 2011; Hatfield et al., 2011; Klady et al., 2011). There are direct and indirect effects of elevated air temperature (T_a) on ecosystem productivity. The direct effects depend on current T_a. In areas with lower T_a, as in boreal climates, warming improves kinetics of carboxylation and hence rates of CO_2 fixation (Bernacchi et al., 2001) due to larger Q_{10} at lower temperatures. However, warming also raises Michaelis–Menten constant for carboxylation, K_c (Bernacchi et al., 2003, 2001) and lowers aqueous CO_2 concentration in canopy chloroplasts, C_c with respect to gaseous CO_2 concentration in canopy leaves, C_i (Farquhar

* Corresponding author.
E-mail address: zmekonne@ualberta.ca (Z.A. Mekonnen).

http://dx.doi.org/10.1016/j.agrformet.2015.11.016
0168-1923/

et al., 1980). Consequently, in areas with higher T_a, as in tropical and subtropical climates, warming with smaller Q_{10} increases photorespiration relatively more than carboxylation (Jordan and Ogren, 1984), and hence causes smaller increases, or even decreases, in rates of CO_2 fixation.

Warming indirectly affects GPP and R_e through alteration of the environment (Shaver et al., 2000). It can have an adverse effect on water relations: warming increases vapor pressure deficits (D), thereby hastening evaporation, transpiration, and soil drying, particularly in warmer climates (Grant et al., 2008). Consequent declines in canopy water potential (ψ_c), induce rises in canopy (r_c) and leaf (r_l) resistances (Grant et al., 1999) and hence declines in rates of CO_2 diffusion and carboxylation, reducing CO_2 fixation. Warming also increases autotrophic maintenance respiration (R_m) which rises continuously with temperature while CO_2 fixation does not, so that rises in R_m increasingly offset those in GPP on net CO_2 fixation with warming. Other indirect effects of warming on GPP occur through hastened decomposition, hence N mineralization (Hart, 2006; Ineson et al., 1998) and root and mycorrhizal N uptake, thereby raising leaf nitrogen concentrations and so increasing CO_2 fixation rates. Warming may also affect GPP by altering species composition and abundance (Hudson and Henry, 2009; Izaurralde et al., 2011; Pieper et al., 2011; Shaver et al., 2000) and may thereby change woody carbon stock.

These direct and indirect effects cause ecosystems to increase GPP relatively more with warming in higher latitudes and cooler regions than in lower latitudes and warmer regions (Shaver et al., 2000). This might be due to greater temperature response of CO_2 fixation and nutrient mineralization when temperature is low and Q_{10} values are larger (Sjögersten and Wookey, 2002). In drier and warmer regions, however, D rises more rapidly with warming, hastening declines in soil water potential (ψ_s), ψ_c and stomatal conductance (g_c), and hence in GPP.

These direct and indirect responses of GPP to warming may also vary with plant functional types and climatic zones. For instance, warming may reduce seasonal carbon fixation of annual plants by hastening phenological advance thereby reducing length of growing season, but may raise seasonal fixation in perennial plants by increasing length of growing season (Grant et al., 2009; Kim et al., 2012; Myneni et al., 1997; Piao et al., 2007; Tucker et al., 2001; Zhu et al., 2012). The same rise in temperature can have different impacts on ecosystem processes in different biomes (Oberbauer et al., 2007) and the responses over time can be different (Peng et al., 2009; Way and Oren, 2010).

To examine these contrasting responses to warming, in this study we first analyzed the spatial and temporal variability and trends of warming and precipitation over the last three decades (1979–2010) in NA using climate data from the North American Regional Reanalysis (NARR) (Wei et al., 2014). We then used a comprehensive mathematical process model, *ecosys* (Grant, 2001, 2014; Grant et al., 2011b) to examine how this variability affected the spatial and temporal changes in GPP and leaf area index (LAI) across different ecological regions (eco-regions) of NA. *Ecosys* was used because the direct and indirect effects of warming on biochemical and physical processes that control CO_2 fixation, as described above, are explicitly modeled. The skill of the model to capture these warming effects on ecosystem productivity at different time steps (hourly, daily, annual and decadal) were shown to be generally high, when rigorously tested against measured fluxes over a wide range of climates across different biomes: e.g. wheat growth under controlled warming (Grant et al., 2011b), natural warming in coastal Arctic tundra in Alaska (Grant et al., 2003), mesic Arctic tundra in Northwest Territories, Canada (Grant et al., 2011a); diverse temperate and boreal forests (Grant et al., 2009, 2010), dry grassland in Mediterranean climate zones (Grant et al., 2012); semi-arid grassland in Lethbridge, Alberta (Grant and Flanagan, 2007; Li et al., 2004). In a more recent study (Grant, 2014), the effects of experimental soil warming on nutrient cycling, particularly N mineralization, hence ecosystem productivity in the Harvard forest mixed deciduous stand were tested.

2. Materials and methods

2.1. Model description

A detailed description of inputs, parameters and algorithms used in *ecosys* can be found (Grant, 2001, 2014) and (Grant et al., 2011b, 2012). However, the general descriptions of the algorithms and parameters that are most relevant to modeling the direct and indirect impacts of warming on GPP as described in the introduction are given below and details of the equations used are given in Appendices A–D of the Supplement.

2.1.1. Direct effects

2.1.1.1. CO_2 fixation. Warming affects GPP directly through its effects on carboxylation (Eqs. C6b and C10a), oxygenation (Eqs. C6d and C10b), K_c (Eqs. C6e, C10d and C10e) and modeled by the Arrhenius functions for light and dark reactions, using parameters developed by Bernacchi et al. (2003) for temperatures from 10 to 40 °C and additional parameters for low and high temperatures inactivation by Kolari et al. (2007) as presented in Grant (2014). CO_2 diffusion is controlled by leaf resistance r_l (Eq. C4) which is calculated from a minimum value r_{lmin} (Eq. C5) for each leaf surface that allows a set ratio for intercellular to canopy gaseous CO_2 concentration $C_{i'}$:C_b to be maintained at CO_2 fixation rate V_c under ambient CO_2 concentration (C_a), irradiance, canopy temperature (T_c), leaf nutrient content and zero ψ_c (Grant et al., 2007a). In areas with lower T_a, warming improves kinetics of carboxylation and hence rates of CO_2 fixation (Bernacchi et al., 2001) due to larger Q_{10} at lower temperatures. However, increasing T_a also raises K_c (Bernacchi et al., 2001, 2003) and lowers C_c with respect to C_i (Farquhar et al., 1980). In areas with lower T_a where Q_{10} is larger, the beneficial effect of warming on carboxylation kinetics is greater than the adverse effects of warming on K_c and C_c. But in areas with higher T_a where Q_{10} is smaller, the beneficial effect of warming may be less than the adverse effects, thereby slowing CO_2 fixation by hastening oxygenation more than carboxylation.

2.1.2. Indirect effects

2.1.2.1. Water relations. Warming affects GPP indirectly by increasing D, hence transpiration demand that lowers ψ_c (Eq. B14) and raises r_c (Eq. B2b), thereby slowing CO_2 diffusion (Eq. C2) (Grant et al., 2008). The impact of D on transpiration is solved through the first-order closure of the energy balance (net radiation R_n (Eq. B1a) latent heat flux LE (Eqs. B1b,c), sensible heat flux H (Eq. B1d), and change in heat storage G). Total energy and water exchange between the atmosphere and the ecosystem is the sum of the exchanges with vegetation, snow, residue (coarse woody, fine non-woody) and ground surfaces. Surface energy and water exchanges are coupled with soil heat and water transfers through the surface residue and soil profile (Eq. D12), including freezing and thawing (Eq. D13), surface runoff vs. infiltration (Eq. D1) and subsurface flows through micro- and macropores (Eq. D7), which determine soil temperatures (T_s) and water contents (θ) (Grant, 2004).

Canopy transpiration (E_c) is coupled with water uptake U (Grant et al., 1999) through a convergence solution for ψ_c at which E_c equals U + change in plant water storage (Eq. B14). During this solution, r_c rises from a minimum value r_{cmin} aggregated by leaf surface area from r_{lmin} (Eq. B2a) at zero ψ_c through an exponential function of canopy turgor potential ψ_t (Eq. B2b) calculated from ψ_c and osmotic water potential ψ_π (Eq. B4). U from the soil to the canopy is determined by the potential difference between ψ_c and ψ_s across

soil Ω_s (Eq. B9) and root Ω_r (Eqs. B10–B12) hydraulic resistances and in each rooted soil layer (Eq. B6) (Grant et al., 2007b). Root resistances are calculated from root radial resistivities (Eq. B10) and from primary (Eq. B11) and secondary (Eq. B12) axial resistivities using root lengths and surface areas from a root system sub-model (Eqs. B13) driven by exchange of nonstructural C, N and P along concentration gradients generated by uptake vs. consumption of C, N and P in shoots and roots (Grant, 1998). By raising D and hence E_c and U, warming lowers ψ_c and hence ψ_t and increases r_c, depending on current ψ_s. Increases in r_c reduce rates of CO_2 diffusion (Eq. C2) (Grant et al., 1999).

2.1.2.2. Nutrient uptake. Soil warming enhances N uptake and hence productivity by hastening soil N mineralization (Eq. A26) and root and mycorrhizal active uptake (Eq. C23) through the Arrhenius function of T_s (Eq. A6) (Grant, 2014). Active uptake of N and P U_{NH_4}, U_{NO_3} and U_{PO_4} is calculated from solutions $[NH_4^+]$, $[NO_3^-]$ and $[H_2PO_4^-]$ at root and mycorrhizal surfaces (Eqs. C23b,d,f) at which uptake equals radial transport by mass flow and diffusion (Eqs. C23a,c,e) from the soil solution (Grant et al., 2007b). Path lengths and surface areas of roots and mycorrhizae used to model uptake are calculated from a root and mycorrhizal growth sub-model driven by exchange of nonstructural C, N and P along concentration gradients generated by uptake vs. consumption of C, N and P in shoots and roots (Grant, 1998). A product inhibition function is included to avoid uptake in excess of nutrient requirements (Eq. C23g).

2.1.2.3. Heterotrophic respiration. Oxidation of dissolved organic carbon (DOC) drives heterotrophic respiration (Eq. A11) (R_m (Eq. A18) + growth respiration (R_g) (Eq. A20)) through the Arrhenius function of T_s. R_m is driven by DOC oxidation through Q_{10} function of T_s (Eq. A19) and R_h remaining from R_m drives R_g (Grant, 2014).

2.2. Model drivers

Model drivers are external variables that influence the state of the ecosystem. In this study, climate, soil, land use/land cover dynamics, CO_2 concentration, nitrogen deposition and disturbance were used as inputs to drive *ecosys* (Table 1). The NARR dataset was produced at the National Oceanic and Land Administration (NOAA) National Center for Environmental Prediction (NCEP) Global Reanalysis (Mesinger et al., 2006). NARR is a combined data and model assimilation product that made use of wide network of observational datasets across the continent (Mesinger et al., 2006). For this study, we used a NARR dataset which was reprojected to $0.25^\circ \times 0.25^\circ$ spatial resolution in geographic latitude/longitude projection made available through the Multi-Scale Synthesis and Terrestrial Model Inter-comparison Project (MsTMIP) (Huntzinger et al., 2013). This dataset extended from 1979 to 2010 with a temporal resolution of 3-h, and was interpolated linearly to 1-h for use in *ecosys*. The NARR variables used to drive *ecosys* were air temperature at 2 m, total precipitation at surface, downward shortwave radiation flux at surface, relative humidity at 2 m and wind speed at 10 m.

The soil dataset used in this study was a Unified North America Soil Map (UNASM) which was a reanalysis product of MsTMIP for NA that was prepared using three different soil databases (Liu et al., 2013). The model was provided with attributes for each soil layer in the dataset, including layer depth, clay/sand fraction, pH, total organic carbon, cation exchange capacity and bulk density. Time-varying land use/land cover was modeled from a dataset for the years 1800–2010 developed by merging historical land cover classification (Hurtt et al., 2006) and 2000/2003 SYNMAP (Jung et al., 2006) land cover classification products (Wei et al., 2014). The atmospheric CO_2 concentration used in the model from 1800 to 1979 was created from GLOBEVIEW-CO_2. For the period before 1979 a reanalysis product of GLOBEVIEW-CO_2, Mauna Loa (MLO) and South Pole (SPO) annual mean concentrations as described in Wei et al. (2014) was used. However, for years after 1979 the GLOBEVIEW data were directly used. Annual nitrogen deposition used in the model for 1800–2010 was derived from Dentener's global atmospheric nitrogen deposition maps in the years of 1860, 1993 and 2050 (Dentener, 2006). The annual variation of nitrogen deposition rate from 1890 to 1990 was controlled by EDGAR-HYDE 1.3 (van Aardenne et al., 2001) nitrogen emission data (Wei et al., 2014). Nitrogen deposition was assumed to increase linearly over the remaining period up to the present (1990–2010).

Disturbance due to fire was introduced as external forcing in the model simulation. Four different data sources for Canada, US and Mexico were harmonized to create a continuous historical fire disturbance dataset. The Canadian wildfire information system dataset was available for 1959–1999. US Land Fire Product is a product from United States Geological Survey (USGS). This dataset indicates historical fire regimes based on vegetation dynamics, fire spread and effects and it contains mean fire return interval and a severity index in the average period between fires under the presumed historical fire regime. Another data source used was Global Fire Emission Database (GFED) (Randerson et al., 2013) which partly used the Moderate Resolution Imaging Spectroradiometer (MODIS) global product that combines satellite information on fire activity and vegetation productivity to estimate a burned area and fire emissions. The datasets have a monthly temporal resolution and are available from 1997 to 2012. NACP Forest Age Maps compiled from forest inventories, historical fire data, satellite data, and images from NASA's Landsat Ecosystem Disturbance Adaptive Processing System (LEDAPS) project at 1 km Resolution for Canada and the US were also applied to forested areas (Pan et al., 2011). The Canadian and US maps were produced from data available in 2004 and 2006, respectively. These different products of fire disturbance were not consistent in spatial and temporal resolutions and were in different data models (point and polygon vectors, and raster). Therefore, the products were all geo-rectified, resampled, interpolated and re-gridded to a $0.25^\circ \times 0.25^\circ$ spatial resolution to make it consistent with the projection and spatial resolution of the other model drivers used in this study.

2.3. Model runs and testing

The simulation spatial domain covered the NA landmass with $0.25^\circ \times 0.25^\circ$ resolution consisting of 51,061 independently simulated grid cells. Model runs for each grid cell were prepared with time varying drivers for a simulation period of 1800–2010. To represent historical weather, NARR data from 1979 to 1993 were randomly distributed to form a 100 years spinup sequence that cycled through 1800–1978. This spinup enabled the model to attain a steady state prior to 1979. Then the real time NARR data were used for the rest of the period (1979–2010) to simulate real time ecosystem productivity as stated in MsTMIP protocol (Huntzinger et al., 2013). The model was initialized with attributes from the soil dataset, and run under dynamic land use/land cover changes, atmospheric CO_2 concentrations, nitrogen deposition and disturbances (Section 2.2; Table 1).

2.3.1. Site scale model testing

Model responses of CO_2 exchange to changes in weather are best tested directly against measurements of CO_2 fluxes. However, these measurements can only be done at a site scale at eddy covariance (EC) flux towers with footprints in order of few km^2 (Houborg and Soegaard, 2004; Sasai et al., 2007), making it difficult to

Table 1
Model drivers and their temporal resolution used to drive *ecosys*.

Model Drivers	Temporal period	Temporal resolution	Data source
Climate	1979–2010	3-hourly	NARR[a]
Soil	One time	One time	UNASM[b] (SSURGO (US) + SLC v3.2 (CA) + HWSD v1.1 (MX))
CO_2	1800–2010	Monthly	Enhanced GlobalView[a]
Nitrogen deposition	1800–2010	Yearly	Enhanced Dentener[a]
Land use change	1800–2010	Yearly	Hurtt's harmonized with SYNMAP[a]

All gridded model inputs had 0.25 × 0.25 spatial resolutions.
[a] MsTMIP model drivers (Wei et al., 2014).
[b] Unified North America Soil Map (Liu et al., 2013).

Table 2
Location of 20 EC sites and mean annual air temperature (MAT) and annual precipitation (P) extracted from corresponding pixels of NARR for 2005.

Site	Ecosystem	Latitude	Longitude	MAT (°C)	Annual P (mm)	EC data reference
CA-Ca3	Young Plantation Site-Douglas Fir	49.5	−124.9	10.2	1999	Krishnan et al. (2009)
CA-Gro	Mature Boreal Mixed Wood	48.2	−82.2	4.4	726	McCaughey et al. (2006)
CA-NS1	Boreal black spruce-burn site	55.9	−98.5	0.0	799	Goulden et al. (2006)
CA-Obs	Old Black Spruce	54.0	−105.1	2.6	614	Krishnan et al. (2008)
CA-Ojp	Old Jack Pine	53.9	−104.7	2.5	536	Kljun et al. (2006)
CA-Qfo	Mature Boreal Forest Site	49.7	−74.3	2.7	933	Bergeron et al. (2008)
CA-SJ3	1975 Harv. Yng Jack Pine	53.9	−104.7	2.5	536	Zha et al. (2009)
CA-TP4	Mature White Pine	42.7	−80.4	10.1	951	Arain and Restrepo-Coupe (2005)
CA-WP1	Black Spruce/Larch Fen	55.0	−112.5	3.6	507	Flanagan and Syed (2011)
US-Ha1	Deciduous broadleaf forest	42.5	−72.2	8.6	1740	Urbanski et al. (2007)
US-Los	Shrub wetland	46.1	−90.0	6.4	937	Sulman et al. (2009)
US-Me2	Mid-aged ponderosa pine forest	44.5	−121.6	7.4	983	Thomas et al. (2009)
US-MMS	Deciduous Broad-leaf Forest	39.3	−86.4	9.5	1245	Schmid et al. (2000)
US-MOz	Transitional zone-hardwood and grassland	38.7	−92.2	14.0	1162	Gu et al. (2006)
US-NR1	Subalpine forest	40.0	−105.6	3.4	506	Monson et al. (2005)
US-Ne2	Mead – irrigated maize-soybean rotation site	41.2	−96.5	11.9	819	Verma et al. (2005)
US-Ton	Oak savanna woodland	38.4	−121.0	16.0	815	Ma et al. (2007)
US-UMB	Arboreal composition of the forest	45.6	−84.7	8.3	800	Gough et al. (2008)
US-Var	Grassland	38.4	−121.0	16.0	815	Ma et al. (2007)
US-WCr	Deciduous broadleaf forest	45.8	−90.1	6.4	839	Cook et al. (2004)

validate regional scale model outputs. However, we compared annual modeled GPP aggregated from hourly values for 2005 in pixels corresponding to the locations of 20 EC flux towers, with annual GPP derived from EC measurements (Table 2) over a broad range of eco-regions (Fig. 1) with different climates and biomes across NA (Table 2). Key responses of modeled vs. EC derived GPP to mean annual T_a (MAT) and precipitation were also compared for 2005. The year 2005 was selected due to data availability for a broader range of EC sites.

2.3.2. Continental scale model testing

At a continental scale, modeled annual GPP was also compared with annual averages of MODIS GPP to assess similarities in spatial patterns in 2002 (drought year) vs. 2005 (normal year). Spatial

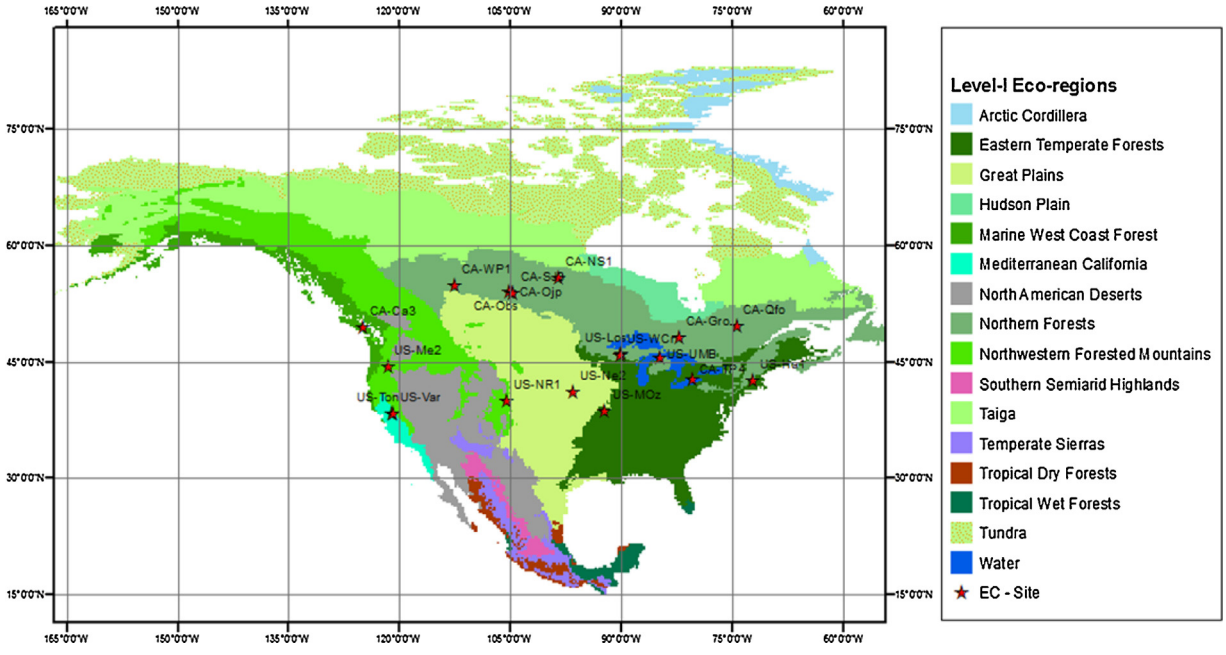

Fig. 1. Level-I eco-regions of North America (Bailey, 1998) and selected eddy covariance sites for model validation.

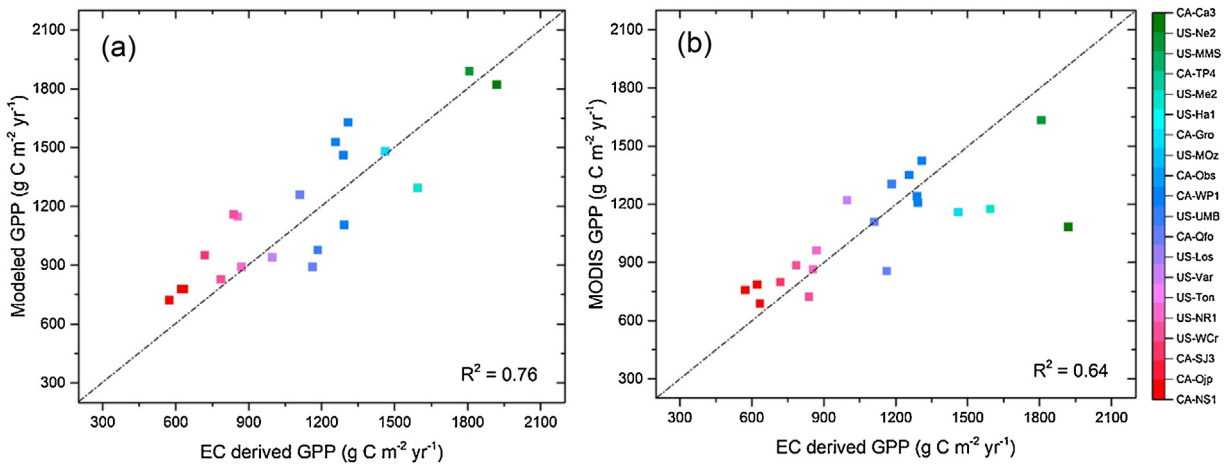

Fig. 2. Correlation between annual GPP for 2005 (a) derived from measurements at 20 selected EC flux tower sites (Table 2) vs. modeled GPP from the corresponding pixels where the EC flux towers were located and (b) EC-derived vs. MODIS GPP averaged for corresponding pixels within 0.25° × 0.25° where the EC flux towers were located.

patterns of average annual (2000–2010) modeled vs. MODIS GPP for NA were tested using geographically weighted regression (GWR). This regression generated separate equations for every spatial cluster in the datasets as a method of analyzing spatially varying relationships. The interannual variability of spatially averaged modeled GPP aggregated to annual totals for NA was compared with that of the MODIS annual GPP product for 2000–2010. Interannual variability of GPP and LAI was also compared with interannual variability in mid-August NDVI from Advanced Very High Resolution Radiometer (AVHRR). Modeled GPP anomalies from the long-term (2000–2010) mean were also compared with those from MODIS.

2.4. Analysis of outputs from continental scale model runs

Three-hourly T_a from NARR and hourly GPP from model outputs for the years 1979–2010 were aggregated to annual averages and totals, respectively, to create continuous gridded data across NA for each year of the study. Model output for mid-August LAI was also extracted. To analyze the long-term temporal trends in T_a and model outputs, the spatial average values were computed considering area of grid cells as a weighing factor. Long-term trends in GPP were done across level I eco-regions of NA with 15 broad eco-region categories (Fig. 1). Long-term spatial and temporal changes in T_a and GPP were computed by subtracting averages of the initial five years of gridded annual values (1980–1984) from those of the final five years (2006–2010). Averaging the initial and final five years was important to smooth out inter-annual variability and detect the long-term spatial and temporal changes of the last three decades. Temporal trends for T_a were also conducted along latitudes and longitudes taking areas of each grid cell as a weighting factor. Disturbances affect productivity in a forest chronosequence (Grant et al., 2007b,c, 2010). Thus, pixels with forest stand age less than 60 years from the last stand replacing fire were excluded from spatial and temporal trend analysis to avoid forest age effects on GPP. Moreover, pixels with forest stands in Mexico were excluded from the trend analysis due to lack of historical disturbance data for the region.

3. Results

3.1. Model testing

3.1.1. Site scale

Annual GPP derived from 20 selected EC site measurements agreed well with modeled GPP from the corresponding pixels where the EC sites were located ($R^2 = 0.76$) demonstrating the ability of the model to simulate CO_2 exchange in wide range of climates and ecosystems across NA (Fig. 2a). Key modeled responses of carbon fixation to differences in MAT and annual precipitation under wider ranges of climates apparent in EC derived GPP were captured in modeled GPP (Fig. 3). Annual CO_2 fixation were shown to be low for EC sites with lower MAT (e.g. <2.6 °C in CA-NS1, CA-SJ3 and CA-Ojp), and increased until the optimum MAT (e.g. 7–10 °C in CA-Ca3, US-Ne2, CA-TP4) was achieved (Table 2; Fig. 3a). Lower annual GPP was observed for EC sites with higher MAT (e.g. >15 °C in US-Var and US-Ton). EC sites with lower annual precipitation (Fig. 3b) were also shown to have low GPP (e.g. US-NR1) and these responses were further pronounced when coupled with higher MAT (Fig. 3).

3.1.2. Continental scale

MODIS GPP tested against EC-derived GPP from 20 EC towers (Fig. 2b) had a good correlation ($R^2 = 0.64$), providing greater confidence to compare the spatial and temporal trends of MODIS against the modeled GPP at continental scale. Long-term (2000–2010) annual modeled vs. MODIS GPP were shown to have similar spatial patterns: higher GPP in south east, Midwest, west coast and southern Mexico (Fig. 4) and lower GPP in the south, southwest and high latitudes. These spatial patterns of modeled vs. MODIS GPP were tested with GWR ($R^2 = 0.8$) which demonstrated close similarities in spatial patterns (Fig. 4). Interannual anomalies in modeled vs. MODIS GPP for NA agreed well showing adverse effects of mid-continental drought in 2002 and drought in the south in 2009 (Fig. 5). Spatial patterns indicated smaller modeled GPP in 2002 for most parts of the southwest and the Great Plains, attributed to the drought compared to a normal year in 2005 (Fig. 6a and b). The spatial patterns of reductions in modeled GPP in the drought affected regions were corroborated by the similar patterns of reduced MODIS GPP in 2002 vs. 2005 (Fig. 6c and d).

3.2. Continental scale: changes in T_a 1979–2010

Changes in T_a derived from the NARR over the last three decades had contrasting regional trends across NA, with some areas at higher latitudes experiencing the most rapid warming while other areas in the western part of the continent were experiencing a slight cooling (Fig. 7a). Average T_a for the entire NA landmass increased by +0.38 °C decade^{-1} from 1979 to 2010, indicating an amplified warming in recent decades (Table 3). Average T_a rose by +0.72 °C decade^{-1} in the northeast including the

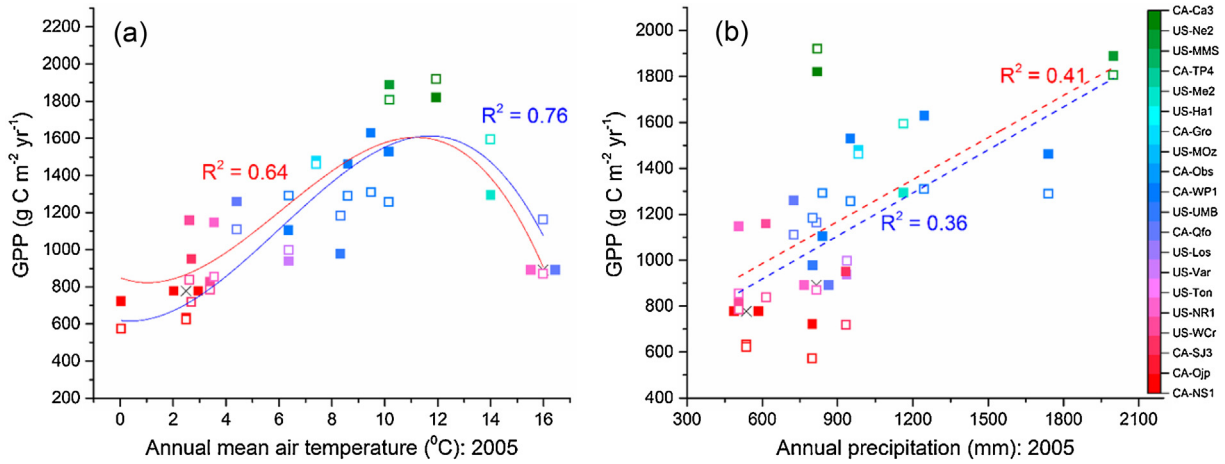

Fig. 3. Relationship between 2005 (a) mean annual air temperature (MAT) and (b) annual precipitation extracted from NARR vs. modeled annual GPP (closed squares) and EC derived annual GPP (open squares) for 20 EC sites across North America. The x symbol represent overlapping points. The regression line and R^2 indicates modeled (red) and EC-derived (blue) GPP. (For interpretation of the references to color in figure legend, the reader is referred to the web version of the article.)

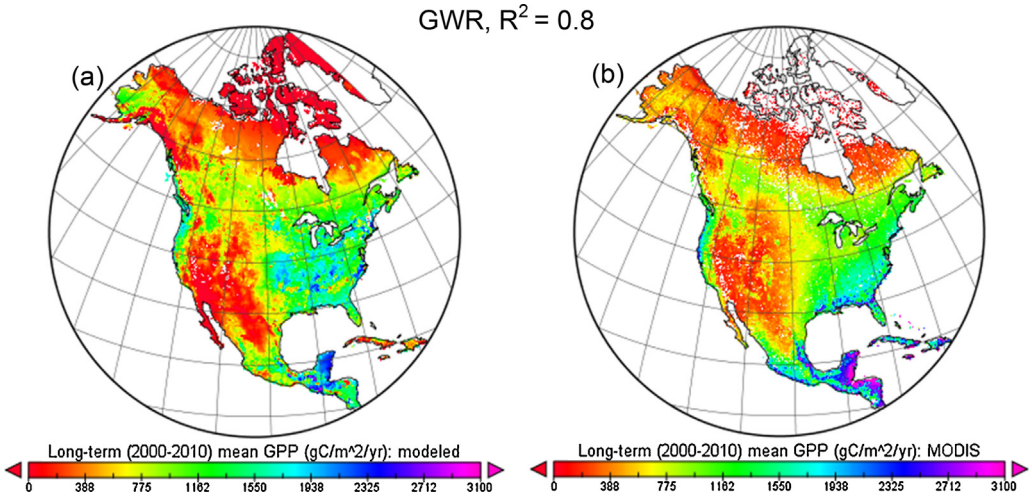

Fig. 4. Long-term (2000–2010) annual average (a) modeled GPP and (b) MODIS GPP for North America.

Canadian Arctic, indicating the most rapid warming at higher latitudes. The western parts of the continent had the slowest warming (+0.08 °C decade^{-1}); with some areas mainly in the northwestern coastal regions experiencing a slight cooling. There were contrasting patterns of warming along latitudinal and longitudinal gradients (Fig. 7c and d). Warming slowed from east to west along spatially averaged longitudes. Regions north of 45° N had more rapid warming of +0.46 °C decade^{-1}, than did regions south of 45° N with +0.19 °C decade^{-1}. Regions between 60° N and 83° N had the most rapid warming, compared to the southern regions except for the small land mass of southern Mexico between 10° N and 15° N.

Seasonal trends in spatially averaged T_a for the entire NA landmass (Table 3) indicated warming in all seasons, however a more pronounced warming of +0.59 °C decade^{-1} was observed in autumn. A slower warming of +0.25 °C decade^{-1} was observed in spring. This result indicated a greater possible increase in length of growing season during late autumn than during early spring in recent decades.

Table 3
Trends in annual and seasonal T_a (°C decade^{-1}) across sub-regions of North America.

Region	Trend (°C decade^{-1})	Latitude	Longitude	Time
Spatial annual average trends in T_a across sub-regions of NA				
North America	0.38	10° N–84° N	50° W–170° W	1979–2010
Northern	0.46	45° N–84° N	110° W–170° W	1979–2010
North east	0.72	51° N–84° N	50° W–170° W	1979–2010
Southern	0.19	10° N–45° N	110° W–170° W	1979–2010
West	0.08	24° N–68° N	110° W–170° W	1979–2010
Spatial seasonal average trends in T_a across NA				
Winter	0.44	10° N–84° N	50° W–170° W	1979–2010
Spring	0.25	10° N–84° N	50° W–170° W	1979–2010
Summer	0.25	10° N–84° N	50° W–170° W	1979–2010
Autumn	0.59	10° N–84° N	50° W–170° W	1979–2010

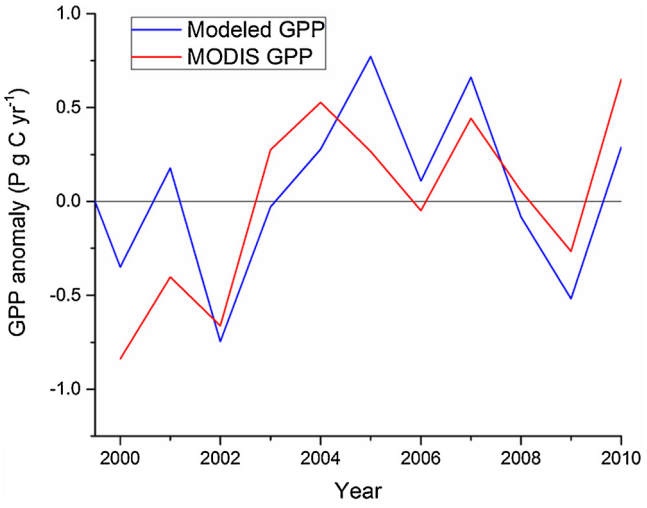

Fig. 5. GPP anomaly for spatial average modeled vs. MODIS GPP from 2000 to 2010 for North America.

Changes in long-term precipitation were more variable than those in T_a across NA (Fig. 7b). Despite the lack of clear spatial trends in precipitation change, most areas at higher latitudes were shown to gain in annual precipitation over the last three decades. Mid and lower latitudes had more spatially variable changes in precipitation. Western coastlines, south western US and southern Mexico had declines in annual precipitation in recent decades.

3.3. Continental scale model runs: changes in GPP 1980–2010

Model results indicated that the different eco-regions of NA varied in their contribution to the total GPP of the continent (Table 4). Productivity was high along the coastlines of northwest and southeast US, south and southeast Mexico (Fig. 8a). Eastern temperate forest, Great Plains and Northern forests contributed most (>60%), accounting for 25%, 18% and 17% of total NA long-term (1980–2010) mean annual GPP, respectively. GPP of tropical forests in parts of southeast Mexico was as much as 3000 g C m^{-2} yr^{-1}. However, ecosystems constrained by temperature such as Arctic cordillera, tundra and those constrained by water such as the deserts in the southwest had the smallest GPP. The GPP contribution of Arctic cordillera and Mediterranean California was less than 1% of the total NA. Spatial variation in productivity was better indicated by the ratios of total productivity to area of each eco-region (Table 4) which varied from 3 g C m^{-2} yr^{-1} for Arctic cordillera to 1802 g C m^{-2} yr^{-1} for tropical wet forests. Spatial variability in LAI was apparent among eco-regions with generally higher values in areas with higher productivity (Fig. 8c).

Percentage of changes in GPP over the last three decades varied among different eco-regions (Table 4). Higher latitude and cooler eco-regions such as Arctic cordillera, tundra, taiga, Hudson plain, northern forests and eastern temperate forest had greater percentage increases in modeled GPP due to early spring and late autumn warming observed in NARR (Table 3). However, declines in GPP were modeled in eco-regions which were already warmer and drier such as North America deserts, temperate sierras, tropical dry forests and Mediterranean California. These eco-regions

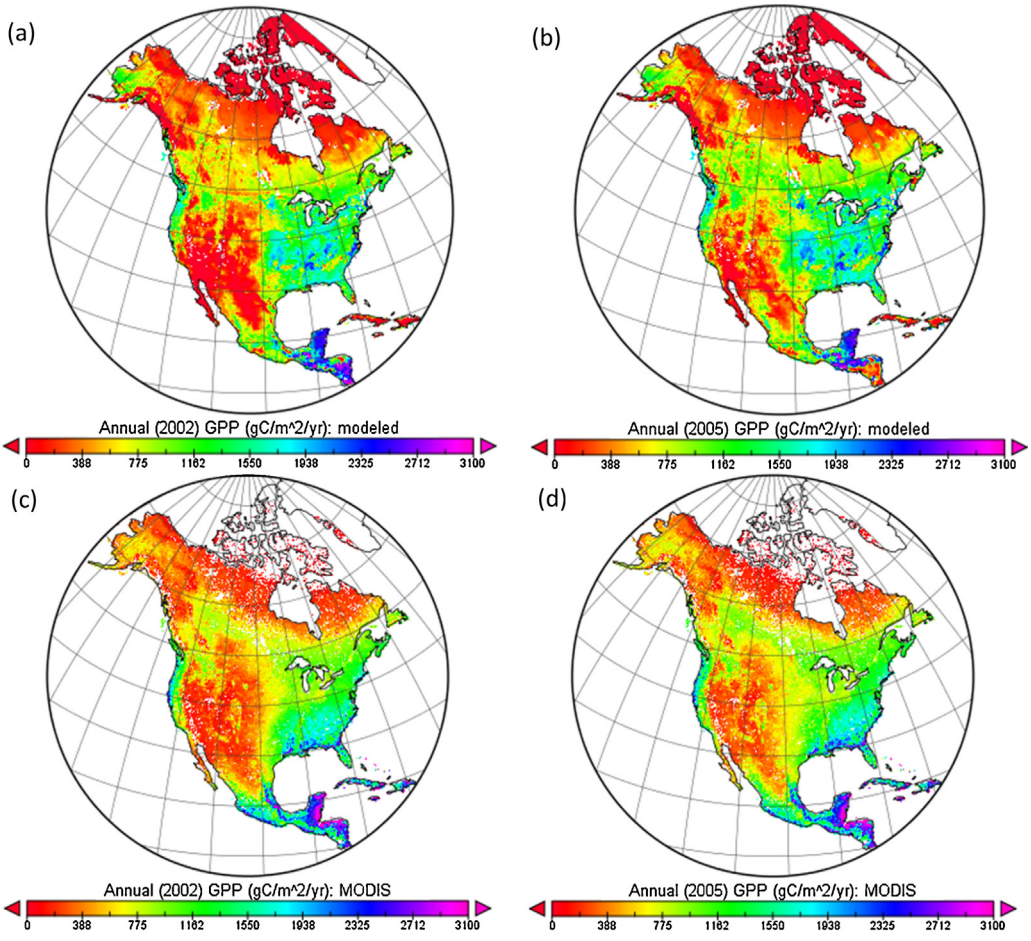

Fig. 6. Comparison of spatial patterns in modeled annual GPP (a, b) and MODIS GPP (b, c) for 2002 (drought) vs. 2005 (non-drought) years for North America.

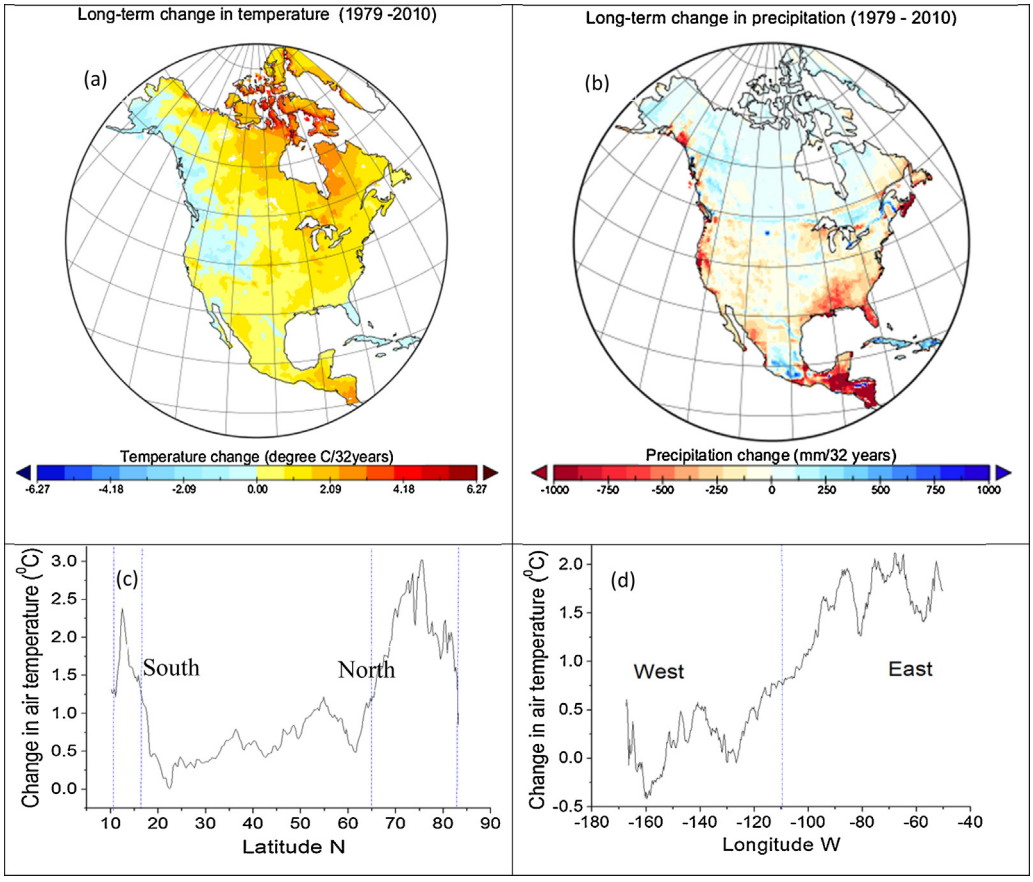

Fig. 7. Long-term (1979–2010) changes in (a) mean annual air temperature, (b) annual precipitation across North America landmass, (c) average air temperature across latitudes, and (d) average air temperature across longitudes.

were mainly in the mid and lower latitudes with higher MAT. Of the total NA landmass about 61% had long-term gains in GPP compared to 23% with long-term losses. The relative contributions of eco-regions to continental carbon uptake vary. Eastern temperate forests, northern forests and Taiga contributed 92% of the increases in NA GPP over the last three decades (Table 3). However, modeled GPP declined in most southwestern regions of NA (accounting >50% of ecosystems with declining GPP) implying that projected dryness in this region (IPCC, 2013) could further reduce NA carbon uptake. Overall, NA modeled GPP increased by 5.8% in the last 30 years, with

Table 4
Long-term (1980–2010) spatial average and changes in modeled GPP, T_a and precipitation across level I eco-regions of North America.

Level I Eco-regions of NA[a]	% GPP[b]	% Area[c]	(GPP/Area)[d]	GPP % change/31 yrs[e]	Changes in T_a/31yrs[f]	Precipitation % change/31 yrs[g]	NA GPP % change[h]
Arctic cordillera	0.01	1.75	3.2	24.2	1.80	14	0.002
North American deserts	3.33	9.04	239	−35.8	−0.03	−21	−1.19
Mediterranean California	0.71	0.79	584	−18.7	0.44	−36	−0.13
Southern semi-arid highlands	1.15	1.27	586	−5.2	0.47	0.3	−0.06
Temperate sierras	3.82	2.63	944	−5.7	0.75	−19	−0.22
Tropical dry forests	1.91	1.59	779	−1.8	0.65	−11	−0.034
Tropical wet forests	4.14	1.49	1803	−0.4	0.83	−22	−0.02
Tundra	3.10	15.97	126	11.0	2.12	20	0.34
Taiga	9.03	13.72	426	21.9	1.07	15	1.98
Hudson plain	1.59	1.69	610	13.3	1.68	0.3	0.21
Northern forests	17.13	13.51	823	21.7	1.26	0.3	3.72
Northwestern forested mountains	8.33	9.52	567	−5.9	−0.08	−4	−0.49
Marine west coast forest	2.68	2.52	688	2.9	−0.69	−7	0.08
Eastern temperate forests	25.16	11.91	1369	6.9	0.92	−12	1.74
Great plains	17.90	12.59	922	−0.5	0.52	−1	−0.09

[a] North America level I eco-regions had 15 broad ecological regions with distinct biological, physical and human characteristics that can be used at regional and continental scale.
[b] Percentage GPP for eco-regions calculated from a long-term (1980–2010) mean GPP map of North America.
[c] Area percentage (area of eco-region/total area of North America).
[d] The ratio of total GPP to the area of eco-regions (g C m^{-2} yr^{-1})
[e] Percentage of GPP change (long-term (1980–2010) change in GPP/long-term mean GPP), positive values indicated an increase in GPP, whereas negative values indicated a decline in GPP.
[f] Change in air temperature (°C 31 yrs^{-1}).
[g] Change in precipitation (mm 31 yrs^{-1}).
[h] Percentage of North America GPP contributed by eco-regions (% GPP[b] × GPP % change/31 yrs[e]).

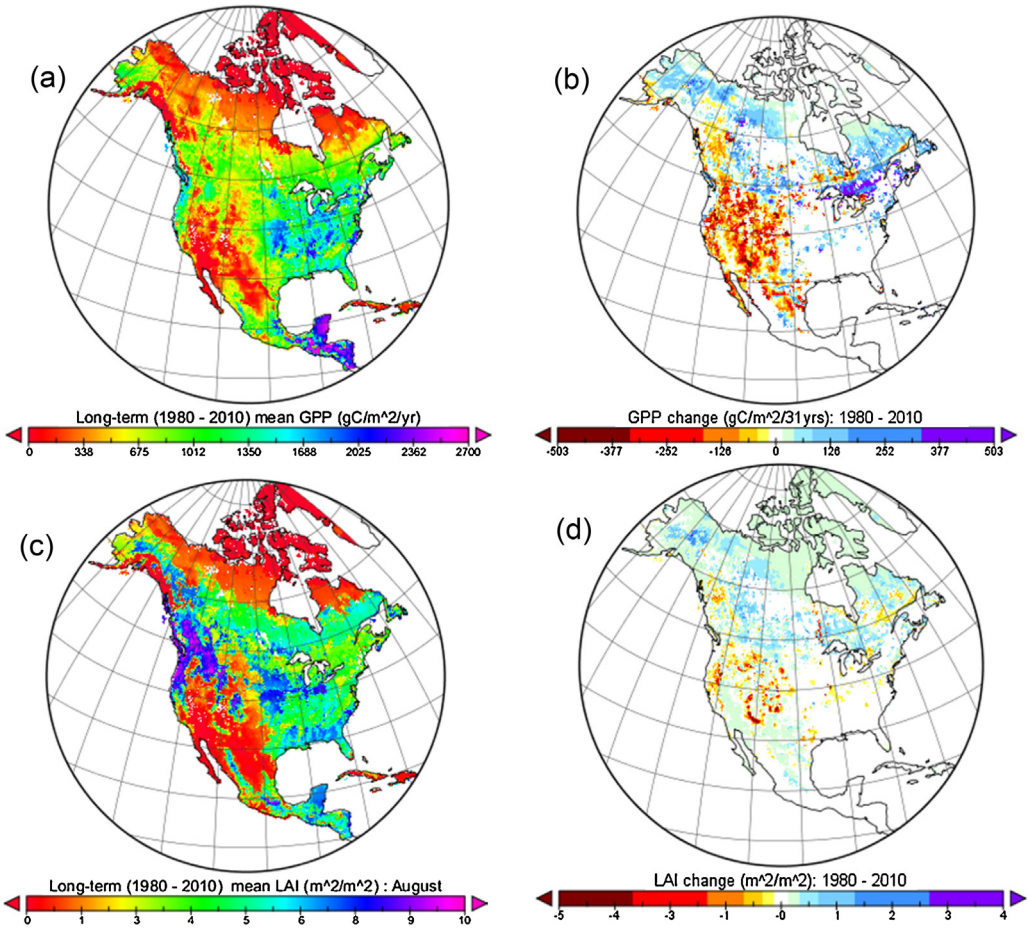

Fig. 8. Long-term mean (a) annual GPP, (c) mid-August LAI and spatially averaged changes average of the first 5 years (1980–1984) subtracted from average of the last 5 years (2006–2010) for (b) annual GPP and (d) mid-August LAI over the last three decades in North America. Pixels with no value in b and d represents forested stands with less than 60 years from the last stand replacing fire and pixels with forest stands in Mexico with no historical disturbance data.

a positive trend of $+0.012 \pm 0.01\,\mathrm{Pg\,C\,yr^{-1}}$ and a range of -1.16 to $+0.87\,\mathrm{Pg\,C\,yr^{-1}}$ caused by interannual variability of GPP from the long-term (1980–2010) mean.

The effects of 30-year changes in T_a and precipitation on modeled GPP differed among regions of NA (Fig. 9). In most northern regions, GPP increased with T_a and less so with precipitation (Fig. 9a). However, in some regions, mainly in Alaska, declines in GPP were caused by slight declines in T_a (Fig. 4a). In most regions of the south and southwest, GPP declined, particularly in regions with rises in T_a and declines in precipitation (Fig. 9b). In a small fraction of the region, GPP rose with increases in precipitation and small changes in T_a. The southeast GPP rose in regions with increased precipitation and declined in those with decreased precipitation, particularly when accompanied by increasing T_a (Fig. 9c). These modeled responses to changes in T_a and precipitation were corroborated by similar responses observed from EC-derived GPP (Fig. 3).

3.4. Continental scale model runs: interannual variability in T_a, precipitation and GPP

Although we could observe long-term trends in continental T_a and precipitation, interannual variation was apparent (Fig. 10a and b) which caused an anomaly range of -1.16 to $+0.87\,\mathrm{Pg\,C\,yr^{-1}}$ in GPP from the long-term mean (Fig. 10c). Despite the apparent long-term positive trend in continental GPP (Fig. 10c), its interannual variability was controlled by that in T_a and precipitation. Significant drops in continental scale modeled GPP were shown by the spatial anomalies from long-term (1980–2010) means during major drought events in 1988 and 2002 (Fig. 10c). This variability was shown spatially by the relative standard deviation (RSD = (standard deviation/absolute value long-term mean) × 100) of modeled annual GPP, mid-August LAI and annual precipitation from the long-term means which varied across the continent (Fig. 11). Those regions which were mainly affected by the droughts during 1988 and 2002, such as parts of the Great Plains, southwest US and northern Mexico had large RSD for GPP and LAI, and precipitation indicating that these parts of the continent had greater interannual variability in productivity and that interannual variability in precipitation control much of the variability on GPP of NA. The Great Plains which contributed 18% of the NA GPP had large RSD demonstrating that this region contributed much of continental scale interannual variability of ecosystem productivity compared to NA deserts and southern semi-arid highlands which had also large RSD but contributed only 3.33% and 1.15% of the total NA GPP, respectively. The coastlines of western Canada and southern Alaska had also large RSD. Interannual variability in modeled carbon fluxes and NARR precipitation was corroborated by similar spatial pattern of interannual variability in mid-August NDVI (Fig. 11d).

4. Discussion

4.1. 30-year spatial and temporal changes in T_a

Our result from analysis of NARR temporal and spatial trends of T_a suggested that most parts of NA have experienced warming in recent decades (Fig. 7a). A particularly amplified warming trend in

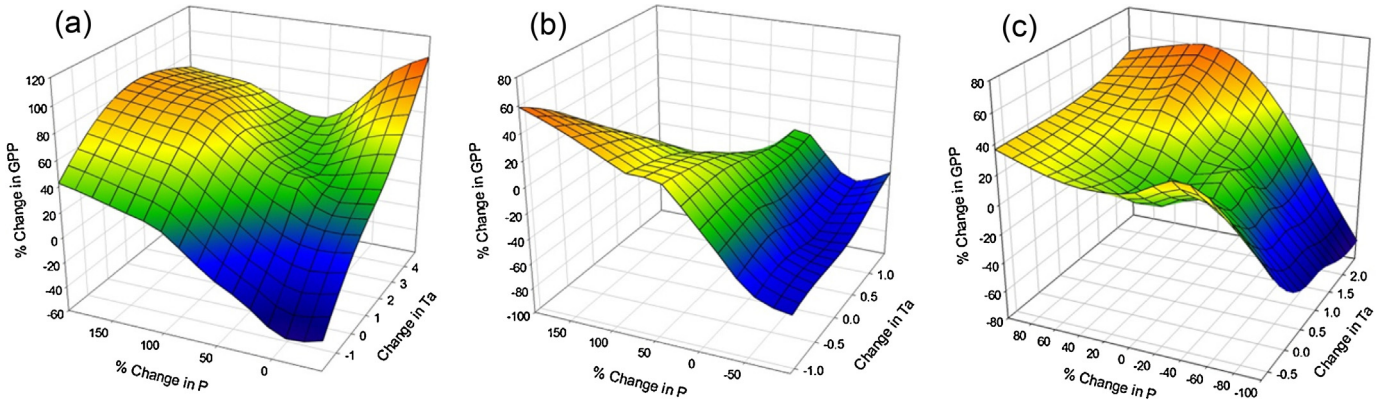

Fig. 9. 3D Mesh graph showing the relationship among long-term (1980–2010) % change in modeled GPP and NARR precipitation (P) and changes in T_a for (a) northern (above 50° N), (b) south and southwest and (c) southeast parts of North America.

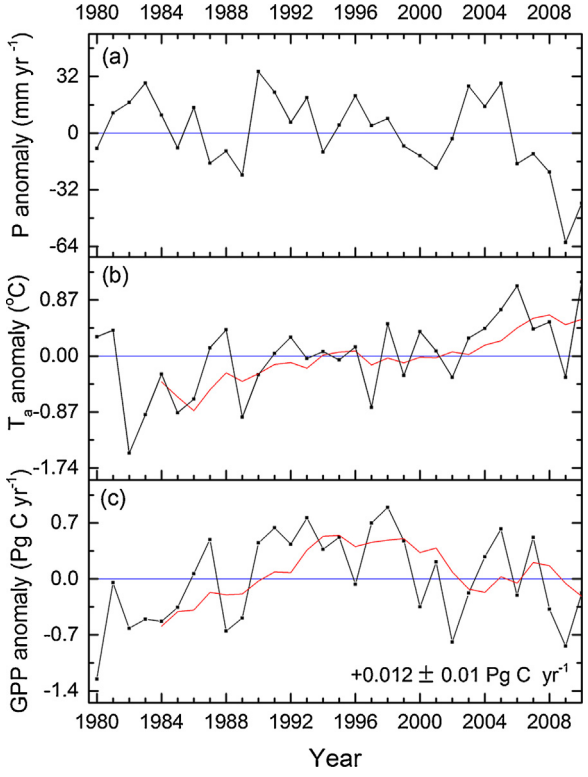

Fig. 10. Anomalies of annual average (a) precipitation, and (b) T_a derived from NARR, and (c) modeled GPP from the long-term mean for North America over the last three decades.

higher latitudes of the northern hemisphere has also been reported in several other studies, although the range of reported warming varied, mainly from different gridded climate datasets. Global increases of +0.04 °C decade^{-1} (1861–1997) and +0.06 °C decade^{-1} (1901–1997) were reported in a study by Jones et al. (1999). Another study covering areas of the Arctic (Polyakov et al., 2002) indicated an increase of +0.17 °C decade^{-1} (1875–2001). An increase of +0.19 °C decade^{-1} in the Arctic was reported for the years 1961–1990 by Chapman and Walsh (1993). A more recent time range (1981–2001) satellite thermal infrared data was shown to have a greater increase of +1.06 °C decade^{-1} in the NA Arctic (Comiso, 2003). The rates of warming were not the same for all seasons although increasing trends of warming were observed in all seasons (Table 3). A winter warming of +1.00 °C decade^{-1} and a cooling of −1.00 °C decade^{-1}, were reported in the eastern and western Arctic Ocean, respectively, from 1979 to 1997 (Rigor et al., 2000). However, spring warming occurred both in the east and the west Arctic and this was partly associated to the Arctic Oscillation mainly in the east (Rigor et al., 2000). A similar longitudinal influence was observed in the NARR with the eastern, particularly the northeast part of NA landmass experiencing a greater warming trend compared to the west (Fig. 7d) which could be attributed to changes in patterns of North Atlantic Oscillation (NAO) (Belkin, 2009). Comiso (2003) reported a positive trend in spring, summer and autumn suggesting recent warming in the Arctic that may be related to changes in phases of Arctic Oscillation and increase in atmospheric greenhouse gases. Similar increases in early spring and late autumn warming (Table 3) observed in NARR had increased modeled GPP (Fig. 8b) in most areas with lower mean annual T_a, such as those in boreal climate zones.

4.2. Uncertainties in continental modeled GPP

In a model-data inter-comparison of 26 models from NACP site synthesis project, modeled vs. EC derived GPP from 39 flux towers across NA demonstrated that *ecosys* performed very well in simulating GPP across a wide range of biomes (correlation coefficient > 0.9) as shown in Fig. 4 of Schaefer et al. (2012). Similarly, we have shown high correlation (R^2 = 0.76) of modeled GPP in 20 selected EC sites (Section 3.1; Fig. 2). However, in this study our simulation used model drivers from coarser resolution gridded inputs for weather and soil that may have affected the accuracy of the estimated GPP.

In an earlier study (Mekonnen et al., 2016) a detailed analysis was conducted of uncertainties in the model estimates associated with model drivers such as NARR and UNASM for six EC sites. CO_2 flux measurements from each site were compared with CO_2 fluxes from the model using gridded vs. measured inputs under contrasting weather (cool vs. warm and wet vs. dry) to analyze differences in modeled NEP. The comparisons indicated that NEP modeled with gridded inputs had less accurate diurnal and seasonal patterns than NEP modeled with inputs from site measurements at some sites, when tested against NEP derived from EC flux measurements. Although differences in NEP were apparent at some sites (e.g. due to shallower soil depth, lack of SON, inaccurate precipitation pattern), key modeled responses of net CO_2 exchange under contrasting weather were nonetheless maintained for most of the sites, supporting their use in the present study. Gridded weather and soil inputs that caused such differences in NEP would certainly affect regional and global carbon budget estimates from models using these inputs, and uncertainties observed in out model outputs are partly attributed to these model inputs.

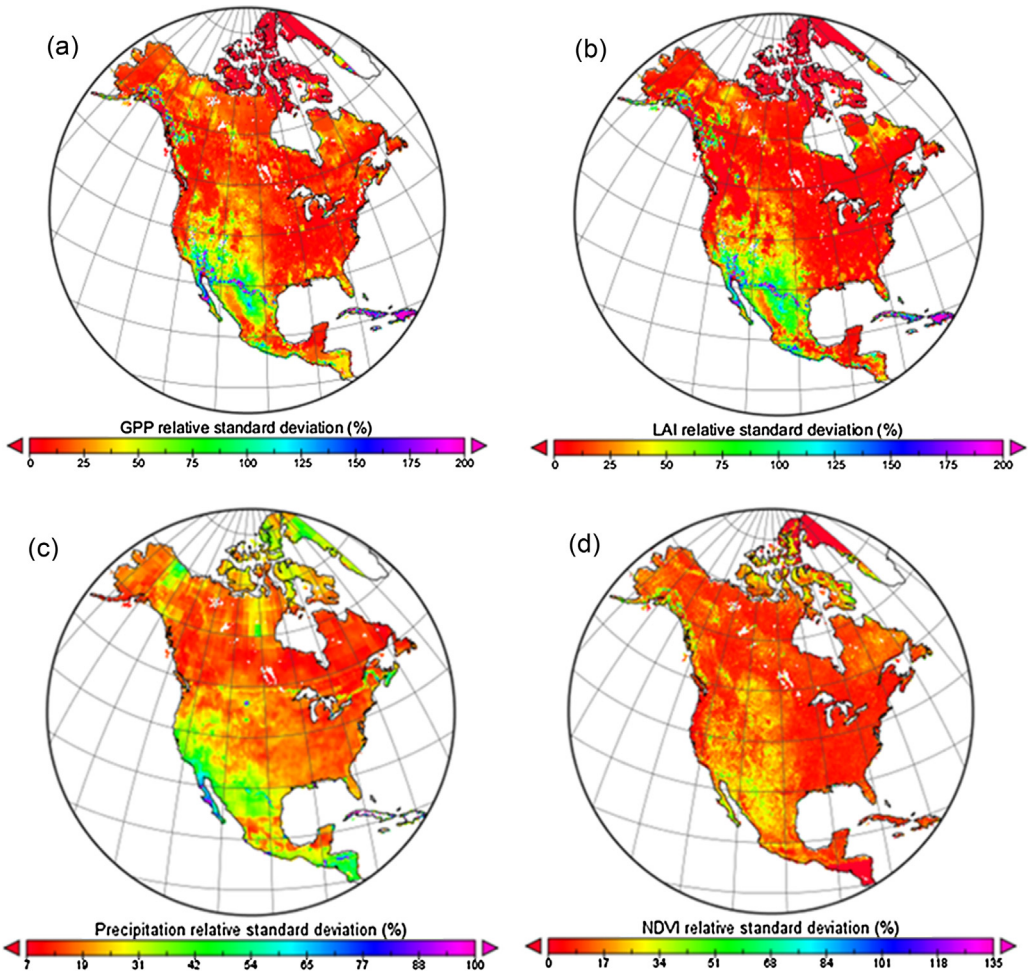

Fig. 11. Long-term (1980–2010) North America (a) GPP relative standard deviation (standard deviation/long-term mean), (b) mid-August LAI relative standard deviation, (c) annual precipitation from NARR relative standard deviation, (d) mid-August NDVI (1982–2006) relative standard deviation.

4.3. Impacts of warming in recent decades on ecosystem productivity

Most parts of NA warmed over the last three decades, although changes in precipitation varied, and the combined effects of changes in T_a and precipitation determined changes in ecosystem GPP in the different climate zones and biomes (Fig. 10). Increases in modeled GPP and LAI in boreal and Arctic ecosystems (Fig. 8b and d) supported the hypothesis that higher latitude and cooler regions tend to have greater relative gains in GPP attributed to warming in recent decades. This is mainly due to temperature responses which are relatively larger in cooler regions where Q_{10} values are larger, but which decline with increasing temperature and declining Q_{10} (Sjögersten and Wookey, 2002), as described in the direct effects of warming modeled in *ecosys* (Section 2.1.1). In these climates warming was mostly coupled with an increase in precipitation (Fig. 7) which increased rates of CO_2 fixation through enhancing kinetics of carboxylation (Bernacchi et al., 2001; Grant et al., 2009), while largely avoiding the indirect effects on CO_2 fixation through declining ψ_s. Furthermore, spring and autumn warming in higher latitude regions observed in NARR (Table 3) increased the length of growing season thereby increasing duration of CO_2 fixation (Grant et al., 2011a). Studies using NDVI have indicated similar increases in length of growing season in higher latitudes of NA (White et al., 2009; Zhu et al., 2012).

The modeled responses of productivity to warming in boreal and Arctic ecosystems in this study were also corroborated by ecosystem responses observed in numerous studies using artificial warming experiments. Some of these experiments reported increases in biomass attributed to warming in the higher latitudes (Hill and Henry, 2011; Klady et al., 2011; Oberbauer et al., 2007). In another test of *ecosys* against experimental warming on wheat growth, Grant et al. (2011b) reported that warming increased wheat yield in cooler weather due to an increase in CO_2 fixation, whereas the same warming decreased wheat yield in warmer weather due to adverse impacts on water status, increases in respiration and shortening of the growing period. In a further test of *ecosys* against an artificial soil warming experiment (Grant, 2014; Melillo et al., 2011) modeled increased forest productivity was caused by more rapid N mineralization, hence uptake. Findings from a long-term (1981–2008) plot study (Hudson and Henry, 2009) were also consistent with the modeled increases in productivity in Canadian high Arctic (Fig. 8b) mainly attributed to warming over the past 30–50 years that resulted in an increase in the length of growing season. Another study (Pouliot et al., 2009) revealed changes in Landsat and AVHRR NDVI from 1985 to 2006 over Canada that showed an increasing trend in the northern regions, demonstrating increases in GPP with warming.

The declines in GPP modeled mainly in areas with high MAT as in NA deserts, Mediterranean California, temperate Sierras and

tropical dry forests (Table 4) were caused by adverse impacts of warming at high T_a on CO_2 fixation (Grant et al., 2008), as described in the direct effects of warming modeled in *ecosys* (Section 2.1.1). These results support the hypothesis that warming in areas of high T_a, as noted in the introduction would result in a decline in productivity. Moreover, a decline in precipitation in these warmer and drier regions coupled with an increase in T_a, caused declines in CO_2 fixation (Table 4), through an indirect effect by hastening transpiration and soil drying as demonstrated in Grant and Flanagan (2007) and described in Section 2.1.2. A study (Williams et al., 2010) that compared tree-ring width data in the southwest forest for the 20th century with long-term climate data reported 18% forest mortality from 1984 to 2008 as a result of increasing warming and aridity. Breshears et al. (2005) reported mortality of over-story trees in southwestern NA woodlands during in 2002–2003 as a result of drought and associated bark beetle infestation that may drive rapid changes in vegetation. Declines in forest density and basal area suggesting increases in tree mortality forests in 76 long-term forest plots in western US, which may be attributed to warming and water deficit in recent decades (Van Mantgem et al., 2009). Changes in forest structure and composition as a result of tree mortality could affect ecosystem functioning, hence ecosystem carbon exchange (Van Mantgem et al., 2009). Drought-induced tree mortality has also been reported in Canadian boreal forests from a study (Peng et al., 2011) that used long-term forest plots and demonstrated an increase in rate of tree mortality over recent decades, suggesting that recent warming and subsequent drought may alter vegetation composition of ecosystems in higher latitudes of NA as in southwestern part of the continent. Projected warming and increases in drought occurrences may increase tree mortality rates, hence ecosystem carbon dynamics. Thus, it is important for ecosystem models to integrate the impacts of tree mortality on ecosystem processes to better understand carbon dynamics during extreme climate events.

Declines in GPP were also modeled in southern Alaska and northwestern Canada (Fig. 8b) from localized declines in precipitation (Fig. 7b) and T_a (Fig. 7a). These declines were similar to one reported by Beck et al. (2011) in which satellite and tree ring data were used to attribute a decline in productivity in the interior Alaska to water stress as a result of warming. Diverse responses of Arctic GPP to warming were inferred in a meta-analysis by Elmendorf et al. (2012) of 61 tundra sites experimentally warmed for up to 20 years in which strong regional variations of plant responses to warming varied with ambient summer temperature, soil moisture and plant functional type.

Despite various contrasting regional responses to warming, it is apparent that projected further warming can have negative feedbacks to productivity, particularly in warmer regions that have already shown such declines. Climate model projections (Seager et al., 2007; Williams et al., 2013) have shown that the southwestern NA will be drier and more arid in the 21st century, indicating further declines in GPP. Similarly, increasing productivity attributed to recent warming, particularly in higher latitudes may not continue indefinitely as further warming may eventually change the general trends of increased continental GPP with warming (Grant et al., 2011a).

4.4. Interannual variability in ecosystem productivity

The greater interannual variability in modeled GPP and LAI observed in south and southwest US, northern Mexico and the Great Plains (Fig. 11) could mainly be attributed to frequent occurrences of El Niño–Southern Oscillation' (ENSO) events that led to major droughts (Herweijer et al., 2007) as in 2002 (Fig. 10c). This variability in modeled GPP was corroborated with MODIS GPP (Fig. 6a and b vs. Fig. 6c and d). Ropelewski and Halpert (1986) reported that declines in NA precipitation from normal patterns were associated to ENSO for western NA and northern Mexico. Interannual variability in CO_2 fluxes were shown to correlate with ENSO events (Jones et al., 2001; Zeng et al., 2005). The interannual variability in anomaly of spatial average annual modeled GPP was corroborated with a similar temporal pattern in the Multivariate ENSO Index (MEI) computed for each of twelve sliding bi-monthly seasons over the last three decades (Fig. 12). Larger positive values of the Multivariate ENSO Index (MEI) indicated El Niño and larger negative MEI indicated La Niña (Wolter and Timlin, 1993, 1998). Smaller modeled GPP during the major droughts in 1988, 2001/02 and 2008/09 (Fig. 12b) was associated with the cold phase of ENSO with large negative MEI (Fig. 12a), indicating that ENSO events control much of the interannual variability of NA GPP.

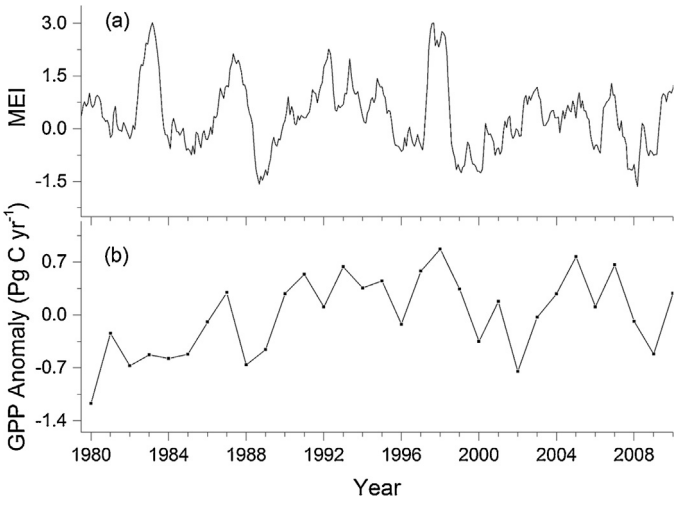

Fig. 12. Interannual variability in (a) anomaly of spatial average annual modeled GPP and (b) Multivariate ENSO Index (MEI) computed for each of twelve sliding bi-monthly seasons over the last three decades (Wolter and Timlin, 1993, 1998).

Greater interannual variability in the south and the prairies could also be attributed to a fast moving low pressure system called 'Alberta Clipper' that moves from southwestern Canada through the Great Plains (Baker et al., 2010). Large interannual variability of sea surface temperature observed in the west of NA in the last century could be associated with changes in coastal ecosystem productivity leading to greater interannual variability (McGowan et al., 1998). Overall continental interannual variability in modeled GPP was most sensitive to interannual variability in the Great Plains, as it contributed 18% of the total GPP of NA, compared to other regions of NA with higher interannual variability in GPP such as the deserts, southern semiarid highlands and temperate sierras that contribute a small fractions for NA GPP. This indicated that impacts of future warming on the Great Plains will most likely have a greater impact on the interannual variability of NA carbon budget.

5. Conclusion

Productivity of ecosystems modeled across NA has shown spatial variability and contrasting responses to warming in recent decades. GPP increased with warming in ecosystems with cooler climates due to an increase in the rate of carboxylation, whereas GPP declined with warming in ecosystems with warmer and drier climates due to adverse impacts on carboxylation and water status associated with higher T_a. Interannual variability was shown to vary spatially across the continent, with greater variability in the southwest US, northern Mexico and the Great Plains that may be

attributed to frequent occurrences of ENSO events that led to major droughts.

Climate projections are showing that global warming is expected to continue as a result of increasing atmospheric CO_2 concentration. Impacts of future warming, under different climate scenarios, on ecosystem productivity are partly uncertain and need to be carefully examined. Gains in GPP modeled and observed as a result of recent warming may not be sustained indefinitely under further warming. In this regard, process-based modeling approach may provide the predictive capability needed to estimate gains and losses of GPP under future climate change scenarios. To this end, model results for changes in CO_2 exchange with those in T_a and precipitation should be tested rigorously against measurements such as those from EC flux towers and plot based studies. It is only through such testing that we can build confidence in projections of ecosystem productivity under future climates.

Acknowledgements

Funding was provided by NSERC Discovery Frontiers (DF) grant through Arctic Development and Adaptation to Permafrost in Transition (ADAPT). We acknowledge the Multi-scale Synthesis and Terrestrial Model Intercomparison Project (MsTMIP; http://nacp.ornl.gov/MsTMIP.shtml) for providing support in environmental driver data. Funding for MsTMIP activity was provided through NASA ROSES Grant #NNX10AG01A. Data management support for preparing, documenting, and distributing model driver and output data was performed by the Modeling and Synthesis Thematic Data Center at Oak Ridge National Laboratory (ORNL; http://nacp.ornl.gov), with funding through NASA ROSES Grant #NNH10AN681. Data products in this study are archived at the ORNL DAAC (http://daac.ornl.gov). Computational facility for *ecosys* was provided by WestGrid supercomputing infrastructure (https://www.westgrid.ca).

Appendix A. Supplementary data

Supplementary data associated with this article can be found, in the online version, at http://dx.doi.org/10.1016/j.agrformet.2015.11.016.

References

Albert, K.R., Mikkelsen, T.N., Michelsen, A., Ro-Poulsen, H., van der Linden, L., 2011. Interactive effects of drought, elevated CO_2 and warming on photosynthetic capacity and photosystem performance in temperate heath plants. J. Plant Physiol. 168 (13), 1550–1561.

Arain, M.A., Restrepo-Coupe, N., 2005. Net ecosystem production in a temperate pine plantation in southeastern Canada. Agric. Forest Meteorol. 128 (3), 223–241.

Bailey, R.G., 1998. Ecoregions Map of North America: Explanatory Note 1548. US Dept. of Agriculture, Forest Service.

Baker, I.T., Denning, A.S., StÖCkli, R., 2010. North American gross primary productivity: regional characterization and interannual variability. Tellus B 62 (5), 533–549.

Beck, P.S.A., et al., 2011. Changes in forest productivity across Alaska consistent with biome shift. Ecol. Lett. 14 (4), 373–379.

Belkin, I.M., 2009. Rapid warming of large marine ecosystems. Prog. Oceanogr. 81 (1–4), 207–213.

Bergeron, O., Margolis, H.A., Coursolle, C., Giasson, M.-A., 2008. How does forest harvest influence carbon dioxide fluxes of black spruce ecosystems in eastern North America? Agric. Forest Meteorol. 148 (4), 537–548.

Bernacchi, C., Singsaas, E., Pimentel, C., Portis Jr., A., Long, S., 2001. Improved temperature response functions for models of Rubisco-limited photosynthesis. Plant Cell Environ. 24 (2), 253–259.

Bernacchi, C., Pimentel, C., Long, S., 2003. In vivo temperature response functions of parameters required to model RuBP-limited photosynthesis. Plant Cell Environ. 26 (9), 1419–1430.

Box, E.O., Holben, B.N., Kalb, V., 1989. Accuracy of the AVHRR vegetation index as a predictor of biomass, primary productivity and net CO_2 flux. Vegetatio 80 (2), 71–89.

Breshears, D.D., et al., 2005. Regional vegetation die-off in response to global-change-type drought. Proc. Natl. Acad. Sci. U. S. A. 102 (42), 15144–15148.

Chapman, W.L., Walsh, J.E., 1993. Recent variations of sea ice and air temperature in high latitudes. Bull. Am. Meteorol. Soc. 74 (1), 33–47.

Comiso, J.C., 2003. Warming trends in the Arctic from clear sky satellite observations. J. Clim. 16 (21), 3498–3510.

Cook, B.D., et al., 2004. Carbon exchange and venting anomalies in an upland deciduous forest in northern Wisconsin, USA. Agric. Forest Meteorol. 126 (3), 271–295.

Dentener, F., 2006. Global Maps of Atmospheric Nitrogen Deposition, 1860, 1993, and 2050. Data Set. Oak Ridge National Laboratory Distributed Active Archive Center, Oak Ridge, TN, USA, Available at: http://daac.ornl.gov.

Elmendorf, S.C., et al., 2012. Global assessment of experimental climate warming on tundra vegetation: heterogeneity over space and time. Ecol. Lett. 15 (2), 164–175.

Farquhar, G., Caemmerer, S., Berry, J., 1980. A biochemical model of photosynthetic CO_2 assimilation in leaves of C 3 species. Planta 149 (1), 78–90.

Flanagan, L.B., Syed, K.H., 2011. Stimulation of both photosynthesis and respiration in response to warmer and drier conditions in a boreal peatland ecosystem. Glob. Change Biol. 17 (7), 2271–2287.

Gough, C., Vogel, C., Schmid, H., Su, H.-B., Curtis, P., 2008. Multi-year convergence of biometric and meteorological estimates of forest carbon storage. Agric. Forest Meteorol. 148 (2), 158–170.

Goulden, M.L., et al., 2006. An eddy covariance mesonet to measure the effect of forest age on land–atmosphere exchange. Glob. Change Biol. 12 (11), 2146–2162.

Grant, R., 1998. Simulation in ecosys of root growth response to contrasting soil water and nitrogen. Ecol. Model. 107 (2), 237–264.

Grant, R., 2001. A review of the Canadian ecosystem model ecosys. In: Modeling Carbon and Nitrogen Dynamics for Soil Management. CRC Press, Boca Raton, FL, pp. 173–264.

Grant, R.F., 2004. Modeling topographic effects on net ecosystem productivity of boreal black spruce forests. Tree Physiol. 24 (1), 1–18.

Grant, R.F., 2014. Nitrogen mineralization drives the response of forest productivity to soil warming: modelling in ecosys vs. measurements from the Harvard soil heating experiment. Ecol. Model. 288, 38–46.

Grant, R.F., Flanagan, L.B., 2007. Modeling stomatal and nonstomatal effects of water deficits on CO_2 fixation in a semiarid grassland. J. Geophys. Res.-Biogeo 112 (G3), G03011.

Grant, R., et al., 1999. Crop water relations under different CO_2 and irrigation: testing of ecosys with the free air CO_2 enrichment (FACE) experiment. Agric. Forest Meteorol. 95 (1), 27–51.

Grant, R.F., Oechel, W.C., Ping, C.L., 2003. Modelling carbon balances of coastal arctic tundra under changing climate. Glob. Change Biol. 9 (1), 16–36.

Grant, R.F., et al., 2007a. Net biome productivity of irrigated and rainfed maize–soybean rotations: modeling vs. measurements. Agron. J. 99 (6), 1404.

Grant, R., Black, T., Humphreys, E., Morgenstern, K., 2007b. Changes in net ecosystem productivity with forest age following clearcutting of a coastal Douglas-fir forest: testing a mathematical model with eddy covariance measurements along a forest chronosequence. Tree Physiol. 27 (1), 115–131.

Grant, R., et al., 2007c. Net ecosystem productivity of boreal jack pine stands regenerating from clearcutting under current and future climates. Glob. Change Biol. 13 (7), 1423–1440.

Grant, R.F., et al., 2008. Changes in net ecosystem productivity of boreal black spruce stands in response to changes in temperature at diurnal and seasonal time scales. Tree Physiol. 29 (1), 1–17.

Grant, R.F., et al., 2009. Interannual variation in net ecosystem productivity of Canadian forests as affected by regional weather patterns – a Fluxnet-Canada synthesis. Agric. Forest Meteorol. 149 (11), 2022–2039.

Grant, R., et al., 2010. Net ecosystem productivity of temperate and boreal forests after clearcutting—a Fluxnet-Canada measurement and modelling synthesis. Tellus B 62 (5), 475–496.

Grant, R.F., Humphreys, E.R., Lafleur, P.M., Dimitrov, D.D., 2011a. Ecological controls on net ecosystem productivity of a mesic arctic tundra under current and future climates. J. Geophys. Res. 116 (G1).

Grant, R., et al., 2011b. Controlled warming effects on wheat growth and yield: field measurements and modeling. Agron. J. 103 (6), 1742–1754.

Grant, R.F., Baldocchi, D.D., Ma, S., 2012. Ecological controls on net ecosystem productivity of a seasonally dry annual grassland under current and future climates: modelling with ecosys. Agric. Forest Meteorol. 152, 189–200.

Gu, L., et al., 2006. Direct and indirect effects of atmospheric conditions and soil moisture on surface energy partitioning revealed by a prolonged drought at a temperate forest site. J. Geophys. Res.: Atmos. 111 (D16), 1984–2012.

Hart, S.C., 2006. Potential impacts of climate change on nitrogen transformations and greenhouse gas fluxes in forests: a soil transfer study. Glob. Change Biol. 12 (6), 1032–1046.

Hatfield, J.L., et al., 2011. Climate impacts on agriculture: implications for crop production. Agron. J. 103 (2), 351–370.

Herweijer, C., Seager, R., Cook, E.R., Emile-Geay, J., 2007. North American droughts of the last millennium from a gridded network of tree-ring data. J. Clim. 20 (7), 1353–1376.

Hill, G.B., Henry, G.H.R., 2011. Responses of High Arctic wet sedge tundra to climate warming since 1980. Glob. Change Biol. 17 (1), 276–287.

Houborg, R.M., Soegaard, H., 2004. Regional simulation of ecosystem CO_2 and water vapor exchange for agricultural land using NOAA AVHRR and Terra

MODIS satellite data. Application to Zealand, Denmark. Remote Sens. Environ. 93 (1–2), 150–167.
Hudson, J.M.G., Henry, G.H.R., 2009. Increased plant biomass in a High Arctic heath community from 1981 to 2008. Ecology 90 (10), 2657–2663.
Huntzinger, D., et al., 2013. The North American Carbon Program multi-scale synthesis and terrestrial model intercomparison project–Part 1: overview and experimental design. Geosci. Model Dev. 6 (6), 2121–2133.
Hurtt, G.C., et al., 2006. The underpinnings of land-use history: three centuries of global gridded land-use transitions, wood-harvest activity, and resulting secondary lands. Glob. Change Biol. 12 (7), 1208–1229.
Ineson, P., et al., 1998. Effects of climate change on nitrogen dynamics in upland soils. 2. A soil warming study. Glob. Change Biol. 4 (2), 153–161.
IPCC, 2013. Climate change 2013: the physical science basis. In: Stocker, T.F., Qin, D., Plattner, G.-K., Tignor, M., Allen, S.K., Boschung, J., Nauels, A., Xia, Y., Bex, V., Midgley, P.M. (Eds.), Contribution of Working Group I to the Fifth Assessment Report of the Intergovernmental Panel on Climate Change. Cambridge University Press, Cambridge, UK/New York, NY, USA.
Izaurralde, R.C., et al., 2011. Climate impacts on agriculture: implications for forage and rangeland production. Agron. J. 103 (2), 371–381.
Jones, P.D., New, M., Parker, D.E., Martin, S., Rigor, I.G., 1999. Surface air temperature and its changes over the past 150 years. Rev. Geophys. 37 (2), 173.
Jones, C.D., Collins, M., Cox, P.M., Spall, S.A., 2001. The carbon cycle response to ENSO: a coupled climate–carbon cycle model study. J. Clim. 14 (21), 4113–4129.
Jordan, D.B., Ogren, W.L., 1984. The CO_2/O_2 specificity of ribulose 1,5-bisphosphate carboxylase/oxygenase. Planta 161 (4), 308–313.
Jung, M., Henkel, K., Herold, M., Churkina, G., 2006. Exploiting synergies of global land cover products for carbon cycle modeling. Remote Sens. Environ. 101 (4), 534–553.
Kim, Y., Kimball, J.S., Zhang, K., McDonald, K.C., 2012. Satellite detection of increasing Northern Hemisphere non-frozen seasons from 1979 to 2008: implications for regional vegetation growth. Remote Sens. Environ. 121, 472–487.
Klady, R.A., Henry, G.H.R., Lemay, V., 2011. Changes in high arctic tundra plant reproduction in response to long-term experimental warming. Glob. Change Biol. 17 (4), 1611–1624.
Kljun, N., et al., 2006. Response of net ecosystem productivity of three boreal forest stands to drought. Ecosystems 9 (7), 1128–1144.
Kolari, P., Lappalainen, H.K., Hänninen, H., Hari, P., 2007. Relationship between temperature and the seasonal course of photosynthesis in Scots pine at northern timberline and in southern boreal zone. Tellus B 59 (3), 542–552.
Krishnan, P., et al., 2008. Factors controlling the interannual variability in the carbon balance of a southern boreal black spruce forest. J. Geophys. Res.: Atmos. (1984–2012) 113 (D9).
Krishnan, P., Black, T.A., Jassal, R.S., Chen, B., Nesic, Z., 2009. Interannual variability of the carbon balance of three different-aged Douglas-fir stands in the Pacific Northwest. J. Geophys. Res.: Biogeosci. (2005–2012) 114 (G4).
Li, T., Grant, R.F., Flanagan, L.B., 2004. Climate impact on net ecosystem productivity of a semi-arid natural grassland: modeling and measurement. Agric. Forest Meteorol. 126 (1), 99–116.
Liu, S., et al., 2013. The Unified North American Soil Map and its implication on the soil organic carbon stock in North America. Biogeosciences 10 (5), 2915–2930.
Ma, S., Baldocchi, D.D., Xu, L., Hehn, T., 2007. Inter-annual variability in carbon dioxide exchange of an oak/grass savanna and open grassland in California. Agric. Forest Meteorol. 147 (3), 157–171.
McCaughey, J., Pejam, M., Arain, M., Cameron, D., 2006. Carbon dioxide and energy fluxes from a boreal mixedwood forest ecosystem in Ontario, Canada. Agric. Forest Meteorol. 140 (1), 79–96.
McGowan, J.A., Cayan, D.R., Dorman, L.M., 1998. Climate-ocean variability and ecosystem response in the Northeast Pacific. Science 281 (5374), 210–217.
McManus, K.M., et al., 2012. Satellite-based evidence for shrub and graminoid tundra expansion in northern Quebec from 1986 to 2010. Glob. Change Biol. 18 (7), 2313–2323.
Mekonnen, Z.A., Grant, R.F., Schwalm, C., 2016. Sensitivity of modeled NEP to climate forcing and soil at site and regional scales: implications for upscaling ecosystem models. Ecol. Model. 320, 241–257.
Melillo, J.M., et al., 2011. Soil warming, carbon–nitrogen interactions, and forest carbon budgets. Proc. Natl. Acad. Sci. U. S. A. 108 (23), 9508–9512.
Mesinger, F., et al., 2006. North American regional reanalysis. Bull. Am. Meteorol. Soc. 87 (3), 343–360.
Monson, R.K., et al., 2005. Climatic influences on net ecosystem CO_2 exchange during the transition from wintertime carbon source to springtime carbon sink in a high-elevation, subalpine forest. Oecologia 146 (1), 130–147.
Myneni, R.B., Keeling, C., Tucker, C., Asrar, G., Nemani, R., 1997. Increased plant growth in the northern high latitudes from 1981 to 1991. Nature 386 (6626), 698–702.
Oberbauer, S.F., et al., 2007. Tundra CO_2 fluxes in response to experimental warming across latitudinal and moisture gradients. Ecol. Monogr. 77 (2), 221–238.
Olthof, I., Pouliot, D., Latifovic, R., Wenjun, C., 2008. Recent (1986–2006) vegetation-specific NDVI trends in northern Canada from satellite data. Arctic 61 (4), 381–394.
Pan, Y., et al., 2011. Age structure and disturbance legacy of North American forests. Biogeosciences 8 (3), 715–732.
Peng, S., Piao, S., Wang, T., Sun, J., Shen, Z., 2009. Temperature sensitivity of soil respiration in different ecosystems in China. Soil Biol. Biochem. 41 (5), 1008–1014.
Peng, C., et al., 2011. A drought-induced pervasive increase in tree mortality across Canada's boreal forests. Nat. Clim. Change 1 (9), 467–471.
Piao, S.L., Friedlingstein, P., Ciais, P., Viovy, N., Demarty, J., 2007. Growing season extension and its impact on terrestrial carbon cycle in the Northern Hemisphere over the past 2 decades. Glob. Biogeochem. Cycles 21 (3).
Pieper, S.J., Loewen, V., Gill, M., Johnstone, J.F., 2011. Plant responses to natural and experimental variations in temperature in Alpine Tundra, Southern Yukon, Canada. Arct. Antarct. Alpine Res. 43 (3), 442–456.
Polyakov, I.V., et al., 2002. Observationally based assessment of polar amplification of global warming. Geophys. Res. Lett. 29 (18), 1878.
Pouliot, D., Latifovic, R., Olthof, I., 2009. Trends in vegetation NDVI from 1 km AVHRR data over Canada for the period 1985–2006. Int. J. Remote Sens. 30 (1), 149–168.
Randerson, J.T., Werf, G.R.v.d., Giglio, L., Collatz, G.J., Kasibhatla, P.S., 2013. Global Fire Emissions Database, Version 3 (GFEDv3.1). Data Set. Oak Ridge National Laboratory Distributed Active Archive Center, Oak Ridge, TN, USA, http://dx.doi.org/10.3334/ORNLDAAC/1191, Available at: http://daac.ornl.gov/.
Rigor, I.G., Colony, R.L., Martin, S., 2000. Variations in surface air temperature observations in the Arctic, 1979–97,. J. Clim. 13 (5), 896–914.
Ropelewski, C.F., Halpert, M.S., 1986. North American precipitation and temperature patterns associated with the El Niño/Southern Oscillation (ENSO). Mon. Weather Rev. 114 (12), 2352–2362.
Sasai, T., Okamoto, K., Hiyama, T., Yamaguchi, Y., 2007. Comparing terrestrial carbon fluxes from the scale of a flux tower to the global scale. Ecol. Model. 208 (2–4), 135–144.
Schaefer, K., et al., 2012. A model-data comparison of gross primary productivity: results from the North American Carbon Program site synthesis. J. Geophys. Res.: Biogeosci. (2005–2012) 117 (G3).
Schmid, H.P., Grimmond, C.S.B., Cropley, F., Offerle, B., Su, H.-B., 2000. Measurements of CO_2 and energy fluxes over a mixed hardwood forest in the mid-western United States. Agric. Forest Meteorol. 103 (4), 357–374.
Seager, R., et al., 2007. Model projections of an imminent transition to a more arid climate in southwestern North America. Science 316 (5828), 1181–1184.
Shaver, G.R., et al., 2000. Global warming and terrestrial ecosystems: a conceptual framework for analysis. Bioscience 50 (10), 871–882.
Sjögersten, S., Wookey, P.A., 2002. Climatic and resource quality controls on soil respiration across a forest–tundra ecotone in Swedish Lapland. Soil Biol. Biochem. 34 (11), 1633–1646.
Sulman, B., Desai, A., Cook, B., Saliendra, N., Mackay, D., 2009. Contrasting carbon dioxide fluxes between a drying shrub wetland in Northern Wisconsin, USA, and nearby forests. Biogeosciences 6 (6), 1115–1126.
Swann, A.L., Fung, I.Y., Levis, S., Bonan, G.B., Doney, S.C., 2010. Changes in Arctic vegetation amplify high-latitude warming through the greenhouse effect. Proc. Natl. Acad. Sci. U. S. A. 107 (4), 1295–1300.
Thomas, C.K., et al., 2009. Seasonal hydrology explains interannual and seasonal variation in carbon and water exchange in a semiarid mature ponderosa pine forest in central Oregon. J. Geophys. Res.: Biogeosci. (2005–2012) 114 (G4).
Tucker, C.J., et al., 2001. Higher northern latitude normalized difference vegetation index and growing season trends from 1982 to 1999. Int. J. Biometeorol. 45 (4), 184–190.
Urbanski, S., et al., 2007. Factors controlling CO_2 exchange on timescales from hourly to decadal at Harvard Forest. J. Geophys. Res.: Biogeosci. (2005–2012) 112 (G2).
van Aardenne, J.A., Dentener, F.J., Olivier, J.G.J., Goldewijk, C.G.M.K., Lelieveld, J., 2001. A 1×1 resolution data set of historical anthropogenic trace gas emissions for the period 1890–1990. Glob. Biogeochem. Cycles 15 (4), 909–928.
Van Bogaert, R., et al., 2011. A century of tree line changes in sub-Arctic Sweden shows local and regional variability and only a minor influence of 20th century climate warming. J. Biogeogr. 38 (5), 907–921.
Van Mantgem, P.J., et al., 2009. Widespread increase of tree mortality rates in the western United States. Science 323 (5913), 521–524.
Verbyla, D., 2008. The greening and browning of Alaska based on 1982–2003 satellite data. Glob. Ecol. Biogeogr. 17 (4), 547–555.
Verma, S.B., et al., 2005. Annual carbon dioxide exchange in irrigated and rainfed maize-based agroecosystems. Agric. Forest Meteorol. 131 (1), 77–96.
Way, D.A., Oren, R., 2010. Differential responses to changes in growth temperature between trees from different functional groups and biomes: a review and synthesis of data. Tree Physiol. 30 (6), 669–688.
Wei, Y., et al., 2014. The North American carbon program multi-scale synthesis and terrestrial model intercomparison project–Part 2: Environmental driver data. Geosci. Model Dev. 7 (6), 2875–2893.
White, M.A., et al., 2009. Intercomparison, interpretation, and assessment of spring phenology in North America estimated from remote sensing for 1982–2006. Glob. Change Biol. 15 (10), 2335–2359.
Williams, A.P., et al., 2010. Forest responses to increasing aridity and warmth in the southwestern United States. Proc. Natl. Acad. Sci. U. S. A. 107 (50), 21289–21294.
Williams, A.P., et al., 2013. Temperature as a potent driver of regional forest drought stress and tree mortality. Nat. Clim. Change 3 (3), 292–297.
Wolter, K., Timlin, M.S., 1993. Monitoring ENSO in COADS with a seasonally adjusted principal component index. In: Proc. of the 17th Climate Diagnostics Workshop, pp. 52–57.

Wolter, K., Timlin, M.S., 1998. Measuring the strength of ENSO events: how does 1997/98 rank? Weather 53 (9), 315–324.
Zeng, N., Mariotti, A., Wetzel, P., 2005. Terrestrial mechanisms of interannual CO_2 variability. Glob. Biogeochem. Cycles 19 (1).
Zha, T., et al., 2009. Carbon sequestration in boreal jack pine stands following harvesting. Glob. Change Biol. 15 (6), 1475–1487.
Zhang, K., et al., 2008. Satellite-based model detection of recent climate-driven changes in northern high-latitude vegetation productivity. J. Geophys. Res. 113 (G3).
Zhu, W., et al., 2012. Extension of the growing season due to delayed autumn over mid and high latitudes in North America during 1982–2006. Glob. Ecol. Biogeogr. 21 (2), 260–271.